Prevention of supercritical carbon dioxide fluid extract from *Chrysanthemum indicum* Linnén on cutaneous squamous cell carcinomas progression following UV irradiation in mice

QI-HONG LUO[1*], HONG-JUAN CHEN[2*], QING-YUAN ZHONG[1*], HAO-EN HE[1], YING-QI HUANG[1], YOU-CHEN LIU[1], BIN LAN[1], YAO-QI WEN[1], SI-LIANG DENG[1], XIAN-HUA DU[1], BAO-QIN LIN[3] and YA-XIAN ZHAN[1]

[1]School of Pharmaceutical Sciences, Guangzhou University of Chinese Medicine, Guangzhou, Guangdong 510006, P.R. China; [2]Department of Pharmacy, The First Affiliated Hospital, Sun Yat-sen University, Guangzhou, Guangdong 510080, P.R. China; [3]Experimental Center, The First Affiliated Hospital of Guangzhou University of Chinese Medicine, Guangzhou, Guangdong 510405, P.R. China

Received October 27, 2023; Accepted April 26, 2024

DOI: 10.3892/etm.2024.12619

Abstract. *Chrysanthemum indicum* Linnén (*C. indicum*), a medicinal and food herb with various bioactive components, may be of beneficial use in cosmetics and the treatment of skin-related diseases. However, to date, few studies have been reported on its potential preventive and therapeutic effects on skin cancer. Therefore, the present study aimed to investigate the effect and potential mechanism of action of supercritical carbon dioxide extract from *C. indicum* (CI_{SCFE}) on UV-induced skin cancer in a mouse model. Kunming mice were allocated randomly to five treatment groups: Sham, model, low concentration CI_{SCFE}, high concentration CI_{SCFE} and positive control nicotinamide groups. The dorsal skin of mice was irradiated with UV light for 31 weeks. Histopathological changes, ELISA assays, immunohistochemical analysis and western blotting were performed to investigate the potential therapeutic effects of CI_{SCFE}. The results showed that CI_{SCFE} alleviated skin oxidative and inflammatory damage in a UV-induced mouse model of skin cancer. Moreover, CI_{SCFE} suppressed abnormal activation of proto-oncogene c-Myc and the overexpression of Ki-67 and VEGF, and increased expression of the anti-oncogene PTEN, thereby reducing abnormal proliferation of the epidermis and blood vessels. Additionally, CI_{SCFE} increased the protein expression levels of NAD-dependent protein deacetylase sirtuin-1 (SIRT1), Kelch-like ECH associated protein 1 (Keap1) and inhibited the expression of nuclear factor 2 erythroid 2-related factor 2 (Nrf2), phosphorylated (p)-p62 (Ser 349), p-p65 and acetyl-p65 proteins in a UV-induced skin cancer mouse model. In summary, CI_{SCFE} exhibited potent anti-skin cancer activity, which may be attributed its potential effects on the p62/Keap1-Nrf2 and SIRT1/NF-κB pathways.

Introduction

Cutaneous cancer is among one of the most common types of cancer as ~1.5 million individuals worldwide are diagnosed with cutaneous cancer annually, accounting for nearly 10% of all new cancer cases (1). Cutaneous squamous cell carcinoma (cSCC) is a common non-melanoma skin cancer that accounts for ~20% of all skin cancers in the United States and UV light is the main causative factor (2,3). The ozone layer absorbs some of the UVB and all of the UVC, so the UV that reaches the Earth's surface is mainly longwave UVA (320-400 nm) and shortwave UVB (280-320 nm) (4). Prolonged exposure to UV radiation generates reactive oxygen species (ROS), which can directly damage DNA, leading to the activation of proto-oncogenes and the inhibition of anti-oncogenes (5). ROS and its modified intermediates can also oxidize proteins, lipids, nucleic acids and carbohydrates, thereby exacerbating metabolic diseases such as obesity, diabetes and dyslipidemia (6,7). In addition, ROS can also activate inflammatory pathways, release inflammatory regulatory factors and further damage DNA (8,9). Genomic instability occurs when DNA damage is not promptly repaired but rather accumulates. If this damage persists, it can eventually lead to the development of cancer (10-12).

Nuclear factor-E2-related factor 2 (Nrf2) is an essential regulator of certain transcription factors involved in oxidative

Correspondence to: Professor Ya-Xian Zhan, School of Pharmaceutical Sciences, Guangzhou University of Chinese Medicine, 223 Waihuan Road, Guangzhou, Guangdong 510006, P.R. China
E-mail: zyx@gzucm.edu.cn

Professor Bao-Qin Lin, Experimental Center, The First Affiliated Hospital of Guangzhou University of Chinese Medicine, 16 Ji Chang Road, Guangzhou, Guangdong 510405, P.R. China
E-mail: linbaoqin@gzucm.edu.cn

*Contributed equally

Key words: *Chrysanthemum indicum* Linnén, UV, skin cancer, NF-κB, nuclear factor 2 erythroid 2-related factor 2

stress. When healthy cells are damaged, a functional defect in the Nrf2 pathway can increase the tumorigenic potential of early tissue damage (13). However, a previous study reported that Nrf2 is continuously abnormally activated during the progression of certain types of carcinoma, including esophageal SCC, cSCC and non-small cell lung cancer (14). He *et al* (15) reported that Nrf2 is involved in a number of metabolic processes in cancer cells, including the pentose phosphate pathway, the regulation of glycolysis and fatty acid metabolism. Aberrant activation of Nrf2 may be associated with the accumulation of p62/sequestosome-1, a multidomain protein that competes with Nrf2 for binding to Kelch-like ECH associated protein 1 (Keap1), which can lead to aberrant Nrf2 activation (16).

Sirtuin1 (SIRT1) is a deacetylase that serves an instrumental role in the inflammatory response. The elimination of SIRT1 in the liver, pancreas and brain results in increased inflammatory responses and ROS accumulation (17). Upregulation of SIRT1 can repair UV-induced DNA injury and photoaging in human immortalized keratinocytes and mouse embryonic fibroblasts (18,19). The physiological functions of SIRT1 are primarily regulated through its deacetylation of co-activators, histones and transcription factors, such as E2F transcription factor 1, c-Myc, FOXO1 and NF-κB (20). SIRT1 inhibits the function of NF-κB by deacetylation of the RelA/p65 subunit, which results in cells entering the TNF-α-mediated apoptotic process (21). *Chrysanthemum indicum* Linnén (*C. indicum*) is a medicinal and food herb, which is readily available in East Asia (22). Previous studies have reported that *C. indicum* may have antihypertensive, antioxidant, antiseptic and anticancer properties, as well as inhibiting lipogenesis (22-25). Supercritical carbon dioxide fluid extraction has been successfully employed for the extraction process of flowers and buds of *C. indicum* because it can ensure a high extraction rate and the structural integrity of its volatile compounds, such as monoterpenes, sesquiterpenes and alkenes (26). A previous study reported that the supercritical carbon dioxide fluid extraction of *C. indicum* (CI_{SCFE}) may show potential for the treatment of liver and brain damage induced by D-galactose in an aging mouse model (22). Moreover, CI_{SCFE} combined with bleomycin was reported to improve the anticancer ability of tumor-transplanted mice and reduce the toxicity of bleomycin (27). Furthermore, CI_{SCFE} inhibited UV-induced photoaging in a mouse model by reducing inflammation and enhancing antioxidant capacity (28). However, the effect of CI_{SCFE} in UV-induced skin carcinogenesis is currently unclear.

The present study aimed to investigate whether local application of CI_{SCFE} could alleviate UV-induced skin cancer in a mouse model through macroscopic, histological and immunohistochemical evaluations, and determine whether CI_{SCFE} could regulate oxidative stress and inflammation related pathways.

Materials and methods

Preparation of CI_{SCFE}. The flowers and buds of *C. indicum* were purchased from Qingping Chinese herbal medicine market of Guangzhou, Guangdong, China, and were identified by Professor Zi-Ren Su of Guangzhou University of Chinese medicine (Guangdong, China). The extraction and identification procedures of CI_{SCFE} were based on previously published literature (27). Briefly, the flowers and buds of *C. indicum* were loaded into the extraction vessel of the 532 Supercritical Fluid Extraction Equipment (Applied Separations). CI_{SCFE} was obtained using an extraction time of 4 h, a pressure of 25 MPa, a temperature of 45˚C and a flow rate of 20 l/h. High-performance liquid chromatography-pulsed amperometric detection (HPLC-PAD) and gas chromatography-mass spectrometry (GC-MS) were used to analyze the chemical composition of CI_{SCFE} (Table SI and Fig. S1). HPLC analysis was performed on a Shimadzu LC40 HPLC system. The separation was performed on a ACE Excel 5 Super C18 column (4.6x250 mm, 5 μm; cat. no. EXL-1211-2546U; Advanced Chromatography Technologies) with a flow rate of 1.0 ml/min, column temperature at 30˚C, and injection volume of 10 μl. The mobile phase consisting of acetonitrile (solvent A) and 0.1% aqueous formic acid (solvent B) was used to elute the targets with the gradient mode (0-5 min: 5% A→25% A; 5-15 min: 25% A→25% A; 15-25 min: 25% A→45% A; 25-35 min: 45% A→55% A; 35-40 min: 55% A→70% A). Luteolin-7-glucoside (cat. no. B20887), luteolin (cat. no. B20888), linarin (cat. no. B20860) and chlorogenic acid (cat. no. B20782) standards were purchased from Shanghai Yuanye Biotechnology Co., Ltd. The content of these compounds was quantitatively analyzed with peak areas under the standard curves at 334 nm. GC-MS analysis was performed on an Agilent 6890-5975 GC-MS system (Agilent Technologies, Inc.). The oven temperature was initially set at 60˚C, then ramped up to 100˚C at a gradient of 10˚C/min (held for 1 min), then to 110˚C at a rate of 1˚C/min (held for 1 min); then to 150˚C at a rate of 3˚C/min (held for 1 min) and finally to 260˚C at a rate of 10˚C/min (held for 5 min). Split injection (0.5 μl) was conducted with a split ratio of 60:1 and helium was used as carrier gas of 1.0 ml/min flow rate. The spectrometer was set to electron impact (EI) mode with an ionization energy of 70 eV, a scanning range of 40-400 amu, and a scanning rate of 0.34 sec/scan. The temperatures of the inlet and ionization source were 230 and 250˚C, respectively. Ultimately, CI_{SCFE} at a concentration of 0.48 mg/cm^2/mouse (low concentration CI_{SCFE}) or 1.6 mg/cm^2/mouse (high concentration CI_{SCFE}) in 10% Tween 80 were used for subsequent animal experiments.

Animal model. A total of 75 specific-pathogen free male Kunming mice (22-24 g, age 8 weeks) were obtained from the Animal Experiment Center, Guangzhou University of Chinese Medicine (Animal Quality Certificate No. 44005800007154). The mice were housed in an environment conforming to the prescribed humidity (50±5%) and temperature (23±2˚C), with food and water *ad libitum* and were maintained under a 12 h light/dark cycle. The laboratory animal license number was SCXK (Yue) 2018-0085 and the ethics certification number was 20190304024. Under the supervision of authorized researchers, all experiments in the present study were approved by the Animal Care and Use Committee of Guangzhou University of Chinese Medicine (approval no. 20190304024; Guangzhou, China) based on the Guidelines for the ethical review of laboratory animal welfare People's Republic of China National Standard GB/T 35892-2018 (29). According to additional markers that may constitute humane endpoints in tumor research, the experimental endpoint for tumor size took into account the fact that UV exposure on the back of mice

causes damage to skin tumors. The experiment was halted when the volume of any of the skin lesions >1,000 mm^3, the maximum diameter >10 mm or when the diameter ≤10 mm but interfered with animal feeding or hindered animal movement. According to the humane endpoint guidance of the present animal experiments, two mice were euthanized, one from the CI_{SCFE}-L group and one from NAA group (30).

Topical CI_{SCFE} treatments and UV exposure. The skin area on the back (2.5x3.0 cm^2) of mice was depilated with a shaver (FS607; FLYCO) (Fig. 1). In our previous study, the concentrations of 0.48 mg/cm^2/mouse and 1.6 mg/cm^2/mouse of CI_{SCFE} reduced skin damage caused by UV exposure (28). Therefore, the mice were randomly allocated to five treatment groups: Sham (no medication or UV radiation), model (only UV radiation without drug treatment), low concentration CI_{SCFE} (0.48 mg/cm^2/mouse), high concentration CI_{SCFE} (1.6 mg/cm^2/mouse) and positive control nicotinamide (NAA; 0.65 mg/cm^2/mouse; Sigma-Aldrich; Merck KGaA) groups. CI_{SCFE} and NAA were applied daily to the shaved area of the skin on the back of the mouse.

Ultra-Vitalux light bulbs were used as a source of UV light (UVA:UVB=93:7; Osram). Mice were positioned 30 cm away from the UV lamp at 23˚C and were irradiated on Mondays, Wednesdays, Fridays and Sundays for 31 weeks. According to our previous study (31), the minimum erythema dose (MED) for mice was 100 mJ/cm^2. UV intensity was 1 MED for the first week and was increased by 1 MED/week until 400 mJ/cm^2 in the 4th week, which was maintained until the end of the experiment. The experiment continued for 31 weeks, with daily observations of mice health and behavior. At 31 weeks, isoflurane (induction, 5%; maintenance, 2%) was used for anesthesia and cervical dislocation was performed on the mice after photographic documentation of the dorsal skin status. Finally, skin tissue from the irradiated area was extracted for subsequent experiments.

Histological analysis. The dorsal skin was fixed in 10% formalin at 26˚C for 48 h. Tissue dehydration was then performed with the following procedure: Soaking in 10% formalin at 26˚C for 1 h, soaked in 75% ethanol at 26˚C for 1.5 h, soaked in 85% ethanol at 26˚C for 1.5 h, soaking in 95% ethanol at 26˚C for 1.5 h, soaking in anhydrous ethanol at 26˚C for 1 h three times, soaking in TO Bio-permeable agent (cat. no. AYA0150; Shanghai Acmec Biochemical Technology Co., Ltd.) at 26˚C for 1.5 h twice and soaking in paraffin wax at 60˚C for 2 h. Subsequently, the tissue was embedded in melted paraffin at 65˚C and sectioned (4 μm). Paraffin sections were stained using Gomori aldehyde fuchsin at 26˚C for 10 min (GAF; cat. no. G1593; Beijing Solarbio Science & Technology Co., Ltd.), hematoxylin and eosin at 26˚C for 20 min (H&E; cat. no. 0619A19; Beijing Leagene Biotechnology Co., Ltd.) and Sirius red staining at 26˚C for 1 h (cat. no. DC0041-100; Beijing Leagene Biotechnology Co. Ltd.). The histological changes in the skin were examined using a light microscope (BX53; Olympus Corporation).

Immunohistochemical analysis. The procedure for fixation, embedding and sectioning of skin tissue is the same as in the *Histological analysis* section. Skin sections (5 μm) were subsequently deparaffinized with the following procedure: Placed in xylene at 26˚C for 10 min three times, in anhydrous ethanol at 26˚C for 5 min and three times, in 95% ethanol at 26˚C for 3 min, in 85% ethanol at 26˚C for 3 min and in 75% ethanol at 26˚C for 3 min. The skin sections were heated in EDTA for 15 min at 95˚C and then the sections were soaked in 3% hydrogen peroxide at 26˚C for 20 min. Tissue sections were then sealed with 10% goat serum (cat. no. SL038; Beijing Solarbio Science & Technology Co., Ltd.) for 30 min at 37˚C. Subsequently, sections were incubated with Ki-67 (1:300; cat. no. ab15580; Abcam) and CD11b (1:4,000; cat. no. ab133357; Abcam) antibodies diluted in PBS at 4˚C overnight. Samples were incubated with anti-rabbit IgG H&L (HRP; 1:1,000; cat. no. ab6721; Abcam) at 37˚C for 1 h, followed by incubation with 3,3-diaminobenzidine at 26˚C for 1 min (cat. no. ZLI-9017; ZSGB-BIO) and counterstaining with hematoxylin at 26˚C for 3 min. Sections were imaged using a light microscope (Olympus Co.; BX53). Samples were semi-quantified using ImageJ software (version 1.53e; National Institutes of Health).

ROS accumulation assay. At week 31, the UV-irradiated dorsal skin of mice was removed and analyzed using a ROS assay. The mouse skin was encapsulated in optimal cutting temperature encapsulant (cat. no. 4583; Sakura Finetek USA, Inc.) and frozen sections (-80˚C; thickness, 8 μm) were incubated with DCFH-DA (cat. no. BB18081; Bestbio) at 37˚C for 30 min. The samples were measured at a wavelength of 525 nm using a fluorescence microscope (BX53; Olympus Corporation). The average fluorescence intensity of ROS was analyzed using ImageJ software (version 1.53e; National Institutes of Health).

Catalase (CAT) and superoxide dismutase (SOD) assays. Skin tissue was homogenized by adding 9 times the volume of saline (g/ml) and the supernatant was collected after centrifugation at 3,000 x g for 10 min at 4˚C. The protein concentration of the supernatant was measured using a BCA kit (cat. no. P0012; Beyotime Institute of Biotechnology). CAT and SOD levels were measured according to the manufacturer instructions of the CAT (cat. no. A007-1; Nanjing Jiancheng Bioengineering Institute) and SOD (cat. no. A001-3; Nanjing Jiancheng Bioengineering Institute) assay kits.

Measurement of 8-hydroxy-2'-deoxyguanosine (8-OHdG), IL-6 and TNF-α. Skin tissues were ground in PBS with a homogenizer (KZ-III-FP; Wuhan Servicebio Technology Co., Ltd.) at 60 Hz for 6 min at 4˚C and subsequently centrifuged at 4˚C and 3,000 x g for 20 min. The supernatant was collected and ELISA kits were used accordingly to the manufacturer's instructions to measure the levels of TNF-α (cat. no. 430904; BioLegend, Inc.), IL-6 (cat. no. 431304; BioLegend, Inc.) and 8-OHdG (cat. no. MM-0221M1; Jiangsu Meimian Industrial Co., Ltd.).

Western blotting. Skin samples were homogenized in RIPA lysis solution (cat. no. P0013B; Beyotime Institute of Biotechnology). Samples were centrifuged at 4˚C and 14,000 x g for 10 min and the protein content was determined using a BCA kit (cat. no. P0010; Beyotime Institute of Biotechnology). The proteins (40 μg/lane) were electrophoresed using a 10% SDS-polyacrylamide gel and transferred

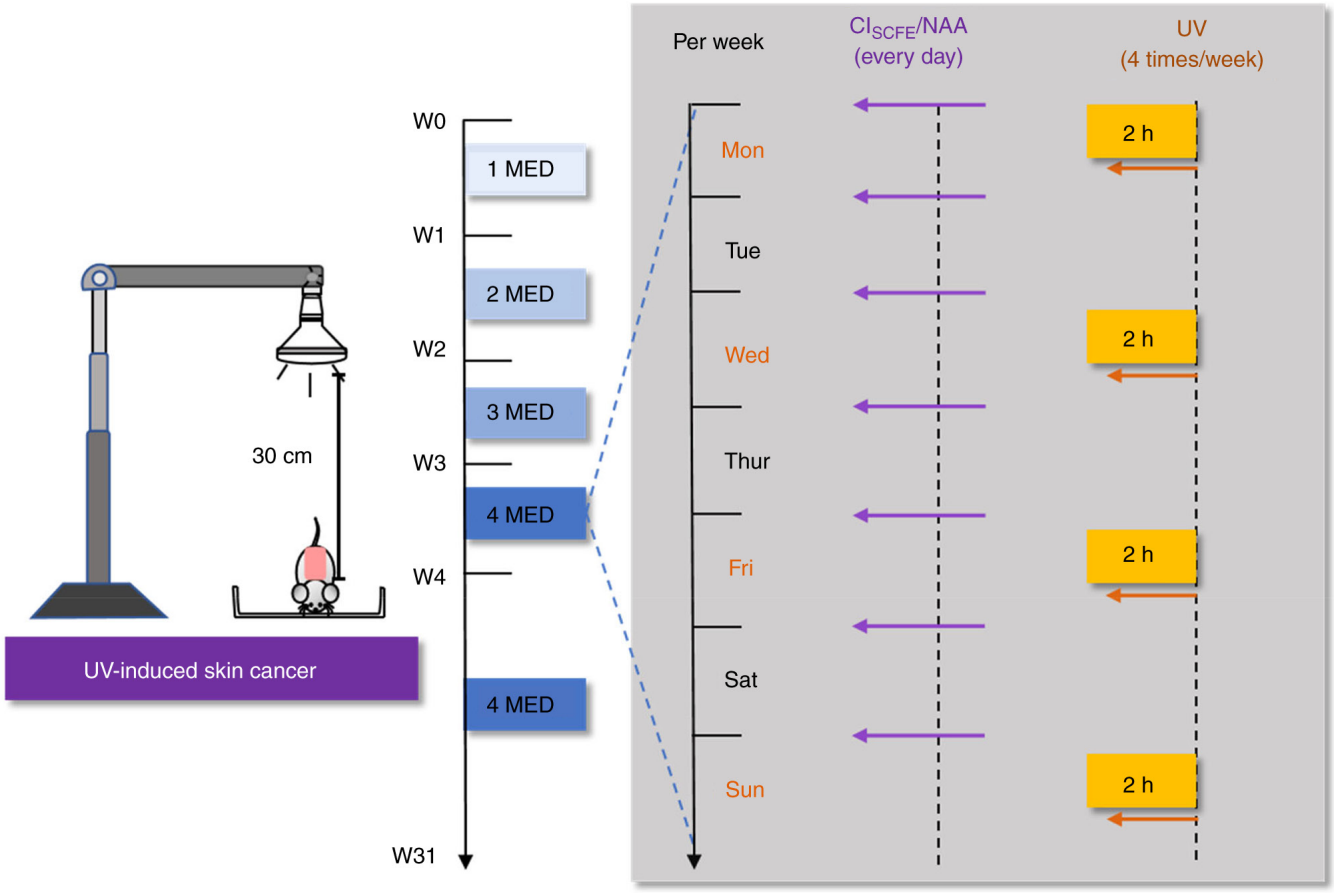

Figure 1. UV irradiation and topical application of CI_{SCFE} during UV-induced skin cancer of mice. Red days of the week indicate when mice were irradiated. W, week; MED, minimum erythema dose; CI_{SCFE}, supercritical carbon dioxide fluid extraction of *Chrysanthemum indicum* Linnén; NAA, nicotinamide.

to PVDF membranes. PVDF membranes were blocked with 5% skimmed milk for 1 h at 26˚C and incubated overnight at 4˚C with heme oxygenase 1 (HO-1; 1:1,000; cat. no. ab13248; Abcam), CD11b (1:1,000; cat. no. ab133357; Abcam), VEGF (1:1,000; cat. no. SC7269; Santa Cruz Biotechnology, Inc.), c-Myc (1:1,000; cat. no. SC40; Santa Cruz Biotechnology, Inc.), p65 (1:1,000; cat. no. 8242S; Cell Signaling Technology, Inc.), PTEN (1:1,000; cat. no. ET1606-43; HUABIO), phosphorylated (p)-p62 (1:1,000; cat. no. ab211324; Abcam), NAD-dependent protein deacetylase sirtuin-1 (SIRT1; 1:1,000; cat. no. ab110304; Abcam), p-p65 (1:1,000; cat. no. ab76302; Abcam), p-IκBα (1:1,000; cat. no. ab133462; Abcam), acetyl-p65 (1:250; cat. no. ab19870; Abcam, IκBα (1:1,000; cat. no. ab32518; Abcam), Nrf2 (1:1,000; cat. no. ab137550; Abcam), NAD(P)H dehydrogenase [quinone] 1 (NQO1; 1:50,000; cat. no. ab80588; Abcam), GAPDH (1:1,000; cat. no. 5174; Cell Signaling Technology, Inc.), lamin B1 (1:2,000; cat. no. AF5161; Affinity Biosciences) and Keap1 (1:2,500; cat. no. ab139729; Abcam) antibodies. Subsequently, membranes were incubated with anti-mouse IgG H&L (1:5,000; cat. no. LK2003; Tianjin Sungene Biotech Co., Ltd.) or anti-rabbit IgG H&L (1:5,000; cat. no. ab6721; Abcam) antibodies for 1 h at 26˚C. Blots were visualized using ECL reagents (cat. no. FD8000; Hangzhou Fude Biotechnology Co., Ltd.) and the blot densities were quantified using ImageJ software (version 1.53e; National Institutes of Health). GAPDH or Lamin B1 were used as loading controls (32).

Statistical analysis. Data were expressed as mean ± standard deviation. Data were analyzed using a one-way ANOVA followed by Tukey's post hoc test. $P<0.05$ was considered to indicate a statistically significant difference. Data were visualized and analyzed using GraphPad software (version 8.3.0; Dotmatics).

Results

Chemical Composition Analysis of CI_{SCFE}. GC-MS analysis and HPLC analysis were used to detect the chemical constituents of CI_{SCFE}. As shown in Table SI, CI_{SCFE} mainly contains d-Camphor, Caryophyllene oxide, Endo-Borneol, α-Curcumene, Cis-verbenol, β-Caryophyllene, Eucalyptol, Thymol as detected by GC-MS. In addition, HPLC analysis detected four compounds in CI_{SCFE} (Fig. S1), which were Chlorogenic acid, Luteolin-7-glucoside, Linarin and Luteolin.

CI_{SCFE} alleviated cutaneous injury induced by UV. Over the course of the present study, it was demonstrated that the skin of the model group showed shallow wrinkles, erythema and a leathery appearance after 9 weeks of UV exposure compared with the sham group (Fig. 2A). The skin in the low dose and high dose CI_{SCFE} groups and the NAA group exhibited no erythema and showed few wrinkles compared with the model group. After 24 weeks of UV irradiation, papular lesions and broken crusts were observed on the skin of model mice. At

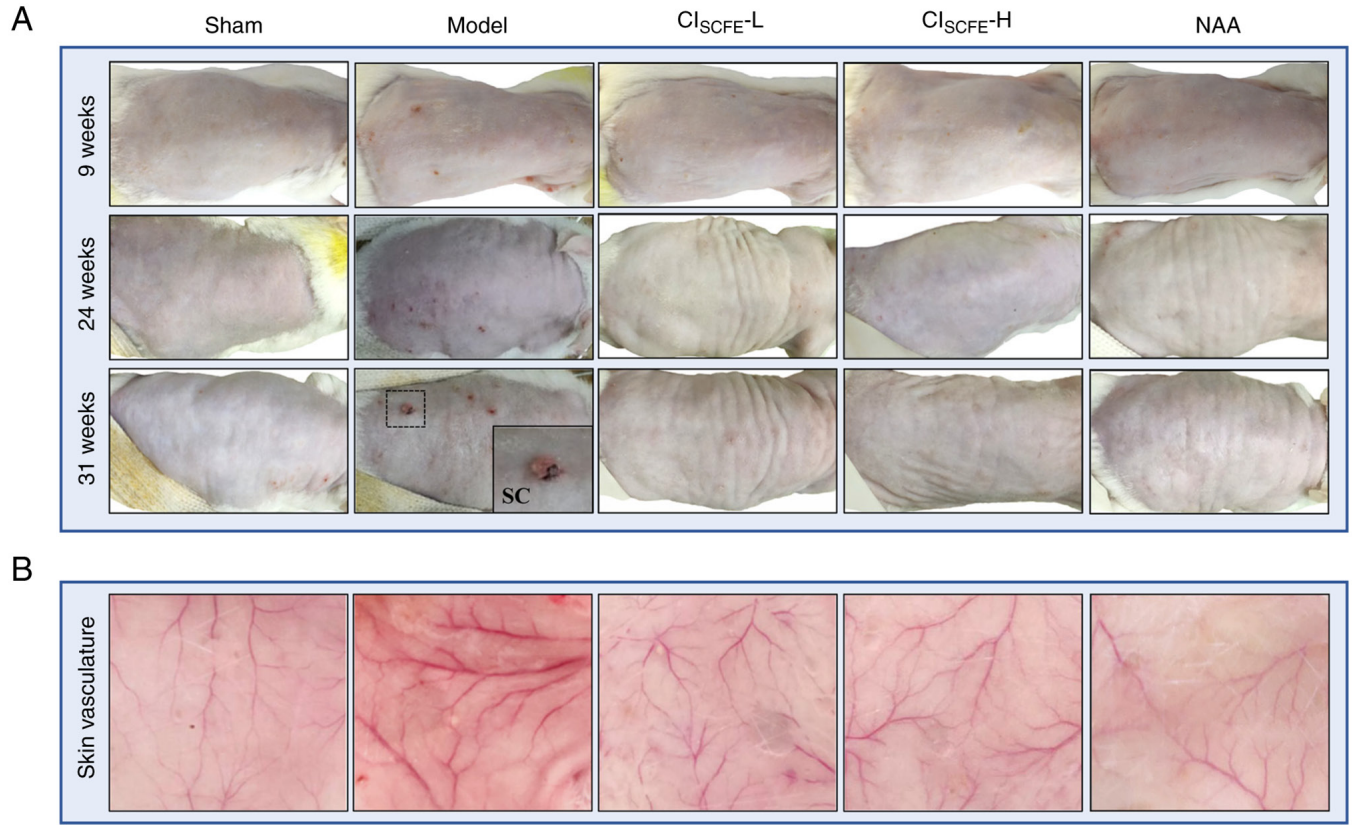

Figure 2. CI$_{SCFE}$ ameliorates UV-induced skin lesions and vascular permeability. (A) Macroscopic images of mouse skin after 9, 24 and 31 weeks of UV irradiation. Highlight, ulcerated erythematous papules with scaling. (B) Dermal blood vessels of mice after 31 weeks of UV irradiation. CI$_{SCFE}$, supercritical carbon dioxide fluid extraction of *Chrysanthemum indicum* Linnén; NAA, nicotinamide; SC, skin cancer; L, low dose; H, high dose; w, week.

week 31, ulcerative papules, adhesive scales, recurrent local bleeding and crusting on the skin was observed on model mice. However, after pretreatment of mice with low or high dose CI$_{SCFE}$ and NAA, there were no papules and deep wrinkles only appeared on the skin at 31 weeks of UV irradiation. Moreover, the dermal vessels in the model group were expanded and proliferated compared with the sham group after 31 weeks of UV irradiation. After pretreatment with CI$_{SCFE}$, at both doses tested, vasodilation and hyperplasia in the dermis caused by UV were markedly reduced (Fig. 2B).

CI$_{SCFE}$ reduced histological damage caused by UV exposure. To observe the histopathologic changes of mouse skin after UV irradiation, GAF, Sirius red and H&E staining were used (Fig. 3A). H&E staining showed that the skin of model mice exhibited abnormal proliferation of the epidermis, keratinocytes extending into the dermis and extensive infiltration of inflammatory cells at week 31. Sirius red and GAF staining of the mouse skin showed that UV irradiation damaged elastic and collagen fibers and reduced their density. Nevertheless, compared with the model group, low and high dose CI$_{SCFE}$ and NAA treatment significantly reduced inflammatory cell infiltration and the deformation and degradation of elastin fibers and collagen fibers and markedly reduced UV-induced abnormal epidermal hyperplasia (Fig. 3B; P<0.01).

CI$_{SCFE}$ inhibited the development of UV-induced skin cancer. To examine the effects of CI$_{SCFE}$ on proliferation, angiogenesis and the expression levels of cancer-related proteins, immunohistochemical assays and western blotting were used to detect Ki-67, VEGF, c-Myc and PTEN expression levels. After 31 weeks of UV irradiation, the epidermis of the model mice exhibited increased Ki-67 expression compared with the sham group (Fig. 4A and B; P<0.001). The epidermal layer in the CI$_{SCFE}$ and NAA groups demonstrated a significant reduction in Ki-67 expression compared with the model group (P<0.001). VEGF and c-Myc protein expression levels were significantly increased and protein expression levels of PTEN were significantly decreased in the model mice compared with the sham group (Fig. 4C-F; P<0.001). After pretreatment with CI$_{SCFE}$ or NAA, VEGF and c-Myc protein expression levels were significantly reduced while PTEN protein expression levels were significantly increased compared with the model group (P<0.05).

CI$_{SCFE}$ suppressed UV-induced oxidative stress and inflammation of skin. To investigate whether the inhibition of skin cancer progression by CI$_{SCFE}$ is related to its antioxidant effects, the levels of ROS, SOD, CAT and 8-OHdG were assayed. An increase in ROS accumulation was observed in the model group compared with the sham group (Fig. 5A and B). However, compared with the model group, CI$_{SCFE}$ and NAA treatment significantly reduced UV-induced ROS overexpression (P<0.05). The activity levels of SOD and CAT were significantly decreased and 8-OHdG was significantly increased in the skin of the model mice at 31 weeks compared

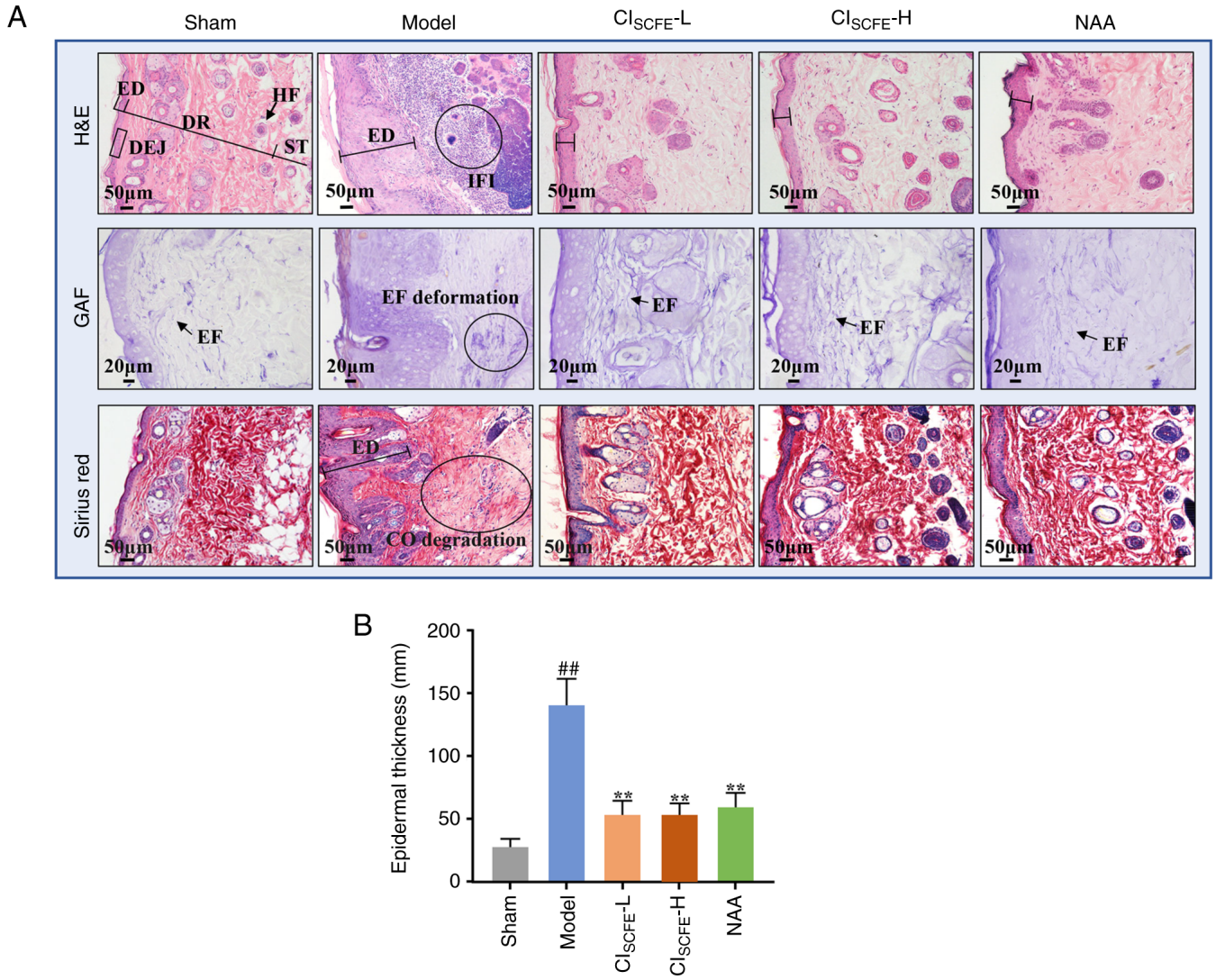

Figure 3. CI$_{SCFE}$ reduces histological damage caused by UV exposure. (A) H&E, (scale bar, 50 μm; magnification, x200), Gomori aldehyde fuchsin (GAF) staining (scale bar, 20 μm; magnification, x400) and Sirius red staining (scale bar, 50 μm; magnification, x200) of mouse skin after 31 weeks of UV irradiation. (B) Epidermal thickness of UV-irradiated mouse skin. Data were expressed as mean ± standard deviation (n=5). $^{\#\#}$P<0.01 vs. sham group; **P<0.01 vs. model group. H&E, hematoxylin and eosin; GAF, Gomori aldehyde fuchsin; ED, epidermis; DR, dermis; DEJ, dermo-epidermal junction; ST, subcutaneous tissue; HF, hair follicle; EF, elastic fiber; CO, collagen; IFI, inflammatory infiltration; CI$_{SCFE}$, supercritical carbon dioxide fluid extraction of *Chrysanthemum indicum* Linnén; NAA, nicotinamide; L, low dose; H, high dose.

with the sham group (Fig. 5C-E; P<0.05). In mice treated with CI$_{SCFE}$ and NAA, the levels of SOD and CAT activity were significantly increased (P<0.05), while 8-OHdG levels were significantly decreased in mice treated with low dose CI$_{SCFE}$ compared with those in the model group (P<0.01).

To explore the level of inflammation in irradiated mouse skin, the expression levels of CD11b, IL-6 and TNF-α were assayed. After 31 weeks of UV irradiation, an increase in CD11b expression was observed in the dermis of model mice compared with the sham group (Fig. 5A and F; P<0.001). The protein expression level of CD11b in the skin of mice treated with CI$_{SCFE}$ and NAA was significantly reduced compared with the model group (Fig. 5G and H; P<0.01). The expression levels of IL-6 and TNF-α in the model group were significantly higher compared with the sham group (Fig. 5I and J; P<0.05). Compared with the model group, topical application of CI$_{SCFE}$ and NAA significantly reduced the expression levels of IL-6 and TNF-α (P<0.05).

CI$_{SCFE}$ prevented UV-induced tumorigenesis by inhibiting Nrf2 and NF-κB pathways. High expression of Nrf2 in tumor cells promotes tumor development (15). Furthermore, NFκB is an important inflammatory and oncogenic transcription factor, and activation of SIRT1 inhibits the NF-κB pathway and suppresses the inflammatory response (21). To explore the potential mechanism of action of CI$_{SCFE}$ against skin cancer in mice, the p62/Keap1-Nrf2 and SIRT1/NF-κB pathway-related proteins were examined. The results showed that the protein expression levels of p62, p-p62, Nrf2, HO-1 and NQO1 were significantly increased, while that of Keap1 significantly decreased in the model group compared with the sham group (Fig. 6; P<0.05). Furthermore, CI$_{SCFE}$ treatment significantly decreased the expression levels of p62, p-p62, Nrf2, HO-1 and NQO1 and significantly increased that of Keap1 compared with the model group (P<0.05). However, the p-p62/p62 ratio was not significantly altered in any treatment condition.

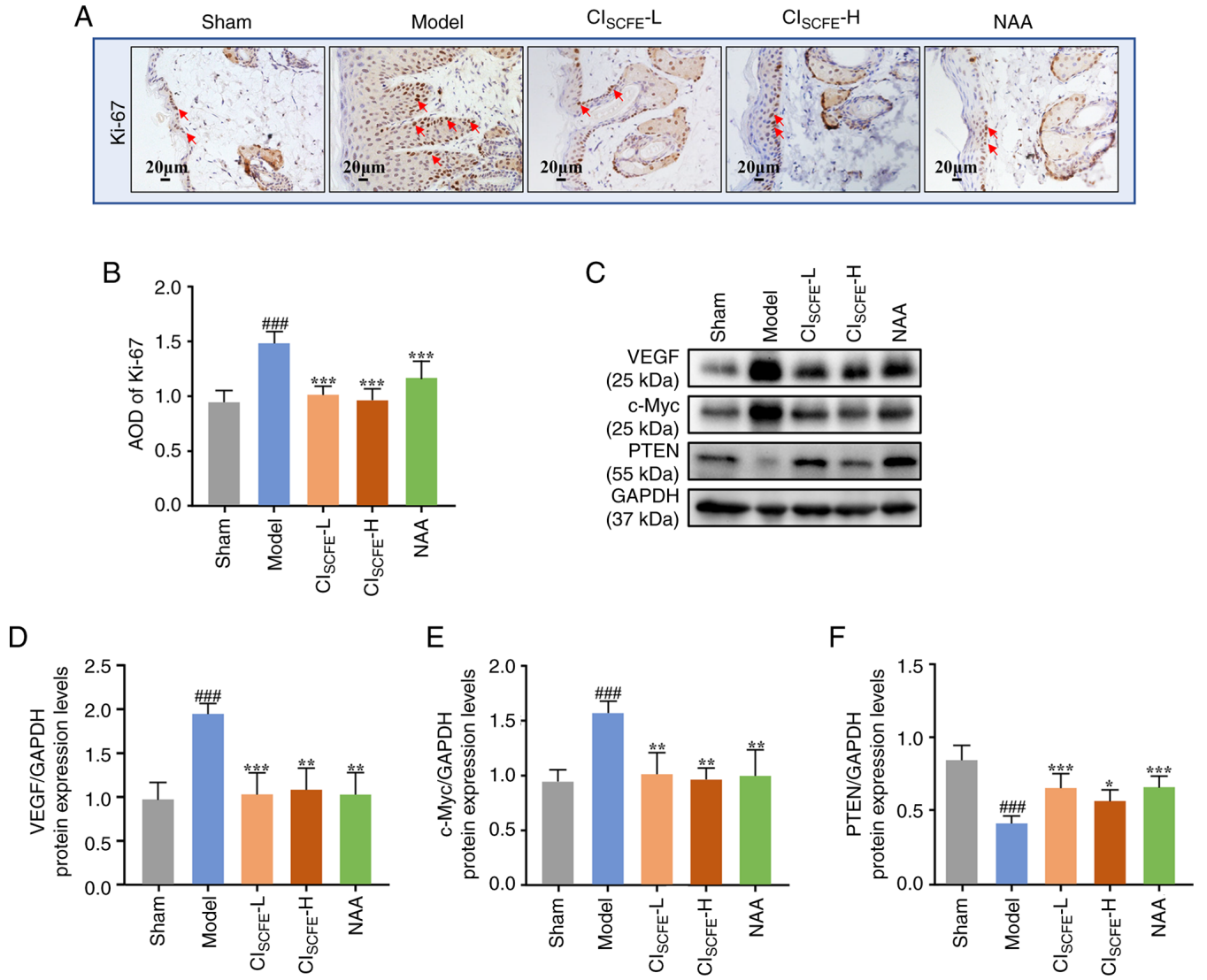

Figure 4. CI$_{SCFE}$ suppresses UV-induced skin carcinogenesis. (A) Immunohistochemical analysis of Ki-67 expression in mice skin at the 31 weeks was conducted on 5 μm sections. Red arrows, expression of Ki-67 in the epidermis; scale bar, 20 μm; magnification, x400. (B) Semi-quantitative analysis of Ki-67 staining. (C) VEGF, c-Myc and PTEN protein expression levels in mouse skin specimens at the 31st week using western blot. Relative changes in protein expression levels intensities of (D) VEGF, (E) c-Myc and (F) PTEN were quantified by densitometric analysis. Data were presented as mean ± standard deviation (n=6). $^{###}$P<0.001 vs. sham group; *P<0.05, **P<0.01, ***P<0.001 vs. model group. CI$_{SCFE}$, supercritical carbon dioxide fluid extraction of *Chrysanthemum indicum* Linnén; NAA, nicotinamide; L, low dose; H, high dose; AOD, average optical density.

Furthermore, there was a significant increase in the protein expression levels of p65, p-p65, acetyl-p65 and p-IκBα in the skin of the model group compared with the sham group (Fig. 7; P<0.05). However, the aforementioned protein expression levels were significantly lower in the CI$_{SCFE}$ group compared with the model group (P<0.05). Additionally, the expression levels of IκBα and SIRT1 were significantly lower in the model group after 31 weeks of UV irradiation compared with the sham group (P<0.01). Topical pretreatment of mice with CI$_{SCFE}$ significantly increased the protein expression level of IκBα compared with the model group (P<0.05). High dose treatment of mice with CI$_{SCFE}$ significantly increased protein expression levels of SIRT1 compared with the model group (P<0.05). Furthermore, p-IκBα/IκBα and p-p65/p65 expression ratios were significantly increased in the model group compared with the sham group (P<0.01). Additionally, p-IκBα/IκBα and p-p65/p65 expression ratios in the skin of CI$_{SCFE}$ mice were significantly decreased compared with the model group (P<0.01).

Discussion

Prolonged exposure to UV radiation can lead to erythema, photoaging, photo immunosuppression and even skin cancer (3). cSCC is a group of skin cancers caused by the malignant growth of epithelial cells, which accounts for 20-50% of skin cancers in the United States (3,33). Although cSCC can be successfully treated surgically, its incidence is still increasing (1). Therefore, it is important to find a drug with low toxicity for prevention and treatment of this condition. It is believed that traditional Chinese herbs have been used for thousands of years to prevent and treat a variety of ailments (34). *C. indicum* is one of these herbs and is used both as a food source and also for the potential prevention

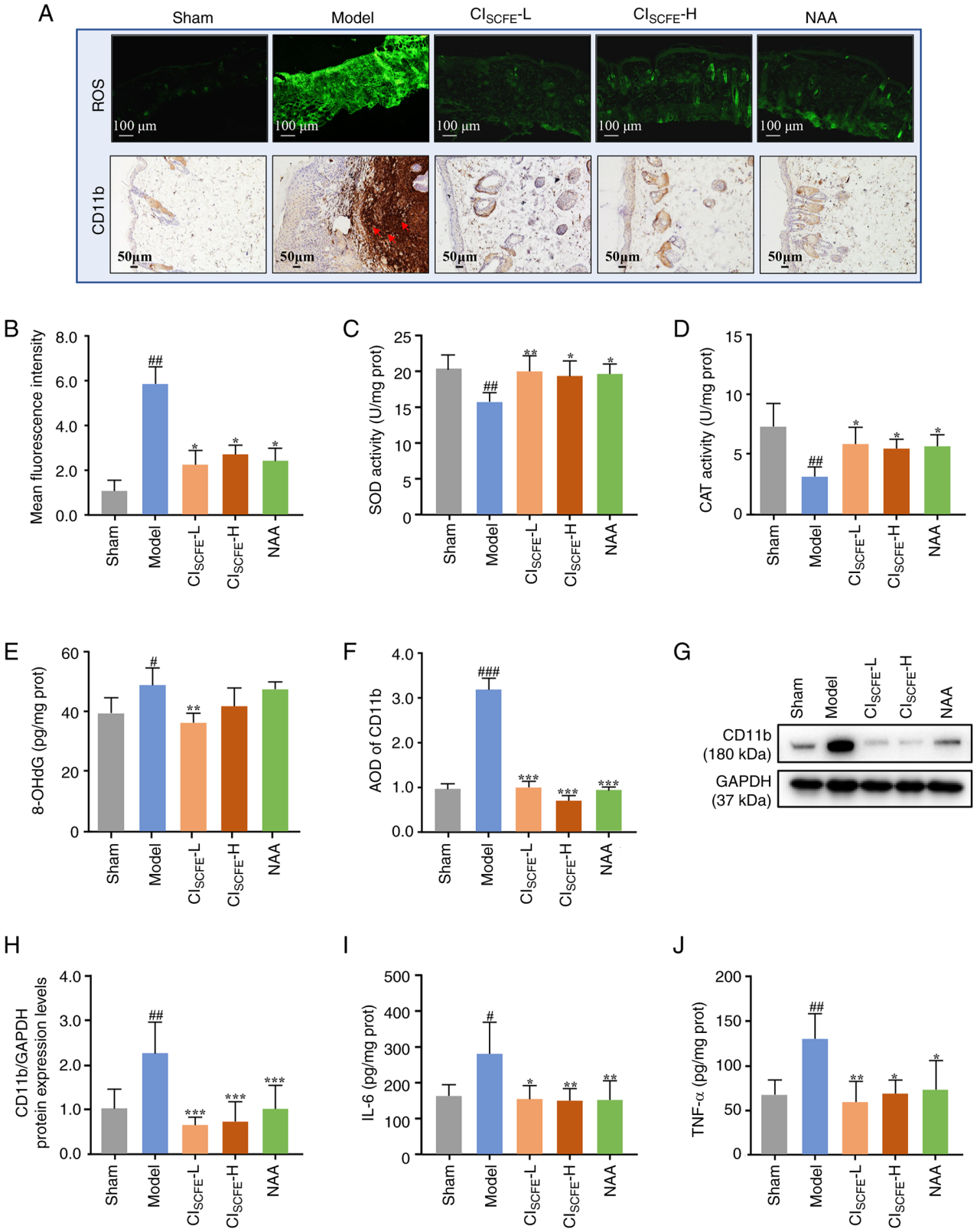

Figure 5. CI$_{SCFE}$ suppresses UV-induced oxidative stress and inflammation in mice. (A) ROS accumulation in mouse skin was assessed by DCFH-DA at week 31. Scale bar, 100 μm; magnification, x100. Green fluorescence represents the intensity of the generated ROS. Immunohistochemical analysis of CD11b expression in mouse skin at week 31 was conducted on 5 μm skin sections (Red arrows, expression of CD11b in dermis; scale bar, 50 μm; magnification, x200). Semi-quantitative analysis of (B) ROS Data were expressed as mean ± SD (n=6). Activity of antioxidant enzymes (C) SOD and (D) CAT activity levels in mouse skin at the 31 weeks were detected using assay kits. Data were presented as mean ± SD (n=8). (E) Levels of 8-OHdG in skin specimens were measured by ELISA kit at 31 weeks. Data were presented as mean ± SD (n=4). Semi-quantitative analysis of (F) CD11b. Data were expressed as mean ± SD (n=6). (G) Analysis of CD11b protein expression levels in mouse skin specimens at 31 weeks using western blotting. (H) Protein expression levels of CD11b were quantified by densitometric analysis. Data were presented as mean ± SD (n=6). Expression levels of (I) IL-6 and (J) TNF-α in skin specimens were measured using ELISA kits at 31 weeks. $^{\#}$P<0.05, $^{\#\#}$P<0.01, $^{\#\#\#}$P<0.001 vs. sham group; *P<0.05, **P<0.01, ***P<0.001 vs. model group. CI$_{SCFE}$, supercritical carbon dioxide fluid extraction of *Chrysanthemum indicum* Linnén; NAA, nicotinamide; L, low dose; H, high dose; AOD, average optical density; ROS, reactive oxygen species; prot, protein, CAT, catalase, SOD, superoxide dismutase; SD, standard deviation; 8-OHdG, 8-hydroxy-2'-deoxyguanosine.

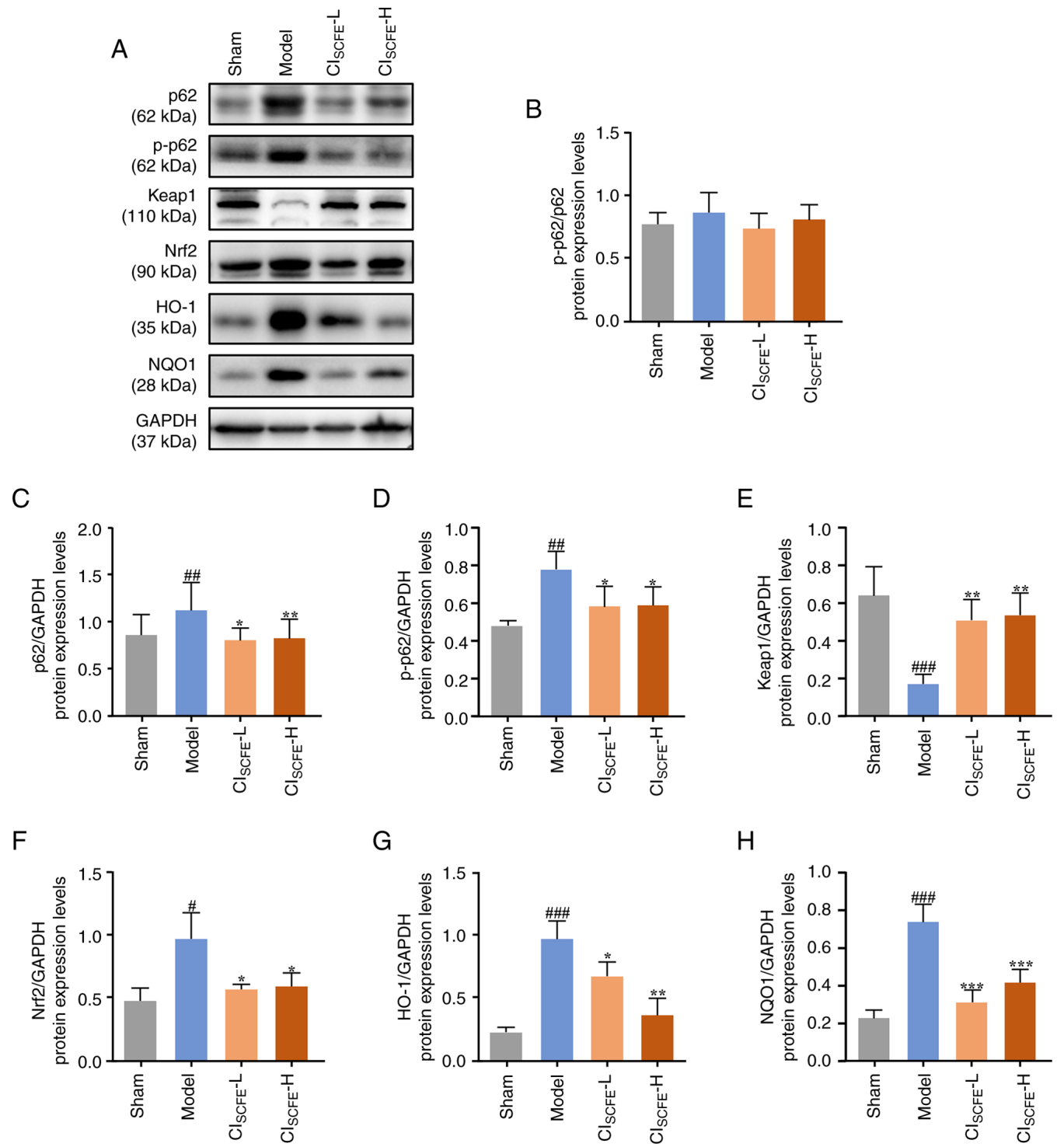

Figure 6. CI_{SCFE} inhibits the UV-induced p62/Keap1/Nrf2 pathway in UV-irradiated mice. (A) Protein expression levels of p62, p-p62, Keap1, Nrf2, HO-1 and NQO1 were analyzed in skin samples at week 31 using western blotting. (B) Quantification of p-p62/p62 in mouse skin. Relative changes in protein expression levels of (C) p62, (D) p-p62, (E) Keap1, (F) Nrf2, (G) HO-1 and (H) NQO1 were quantified by densitometric analysis. Data were presented as mean ± standard deviation (n=4). $^{\#}$P<0.05, $^{\#\#}$P<0.01, $^{\#\#\#}$P<0.001 vs. sham group; *P<0.05, **P<0.01, ***P<0.001 vs. model group. CI_{SCFE}, supercritical carbon dioxide fluid extraction of *Chrysanthemum indicum* Linnén; NAA, nicotinamide; L, low dose; H, high dose; p, phosphorylated; Keap1, Kelch-like ECH associated protein 1; Nrf2, nuclear factor-E2-related factor 2; HO-1, heme oxygenase 1; NQO1, NAD(P)H dehydrogenase [quinone] 1.

and treatment of skin-related diseases (24,34). In the present study, a mouse model of UV-induced skin cancer was used to investigate the potential chemoprevention effect and mechanism of action of *C. indicum* on skin cancer. A number of previous studies have reported the effect of NAA in the field of dermatology and its actions in preventing photoaging and skin cancers in humans (35-37). Moreover, studies have reported that NAA prevented UV radiation from reducing ATP levels and inhibiting glycolysis, thus preventing the UV radiation-induced energy crisis in cells (36,37). Therefore, NAA was used as a positive drug control in the present study to evaluate the anti-skin cancer effect of CI_{SCFE}.

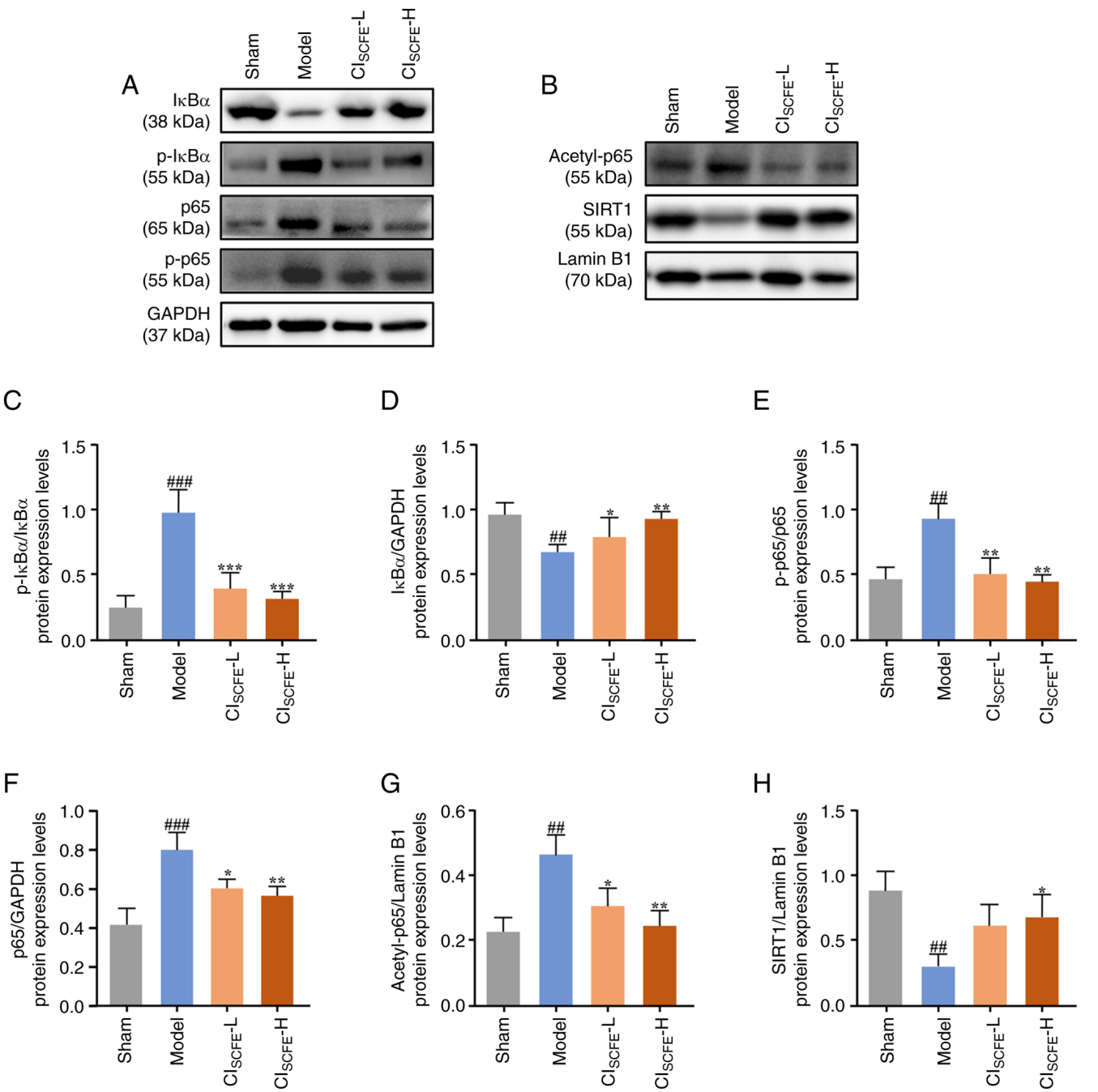

Figure 7. CI_{SCFE} affects the SIRT1/NF-κB pathway in UV-irradiated mice. Protein expression levels of (A) IκBα, p-IκBα, p65, p-p65 and (B) acetyl-p65 and SIRT1 were analyzed in mouse skin samples at 31 weeks using western blotting. (C) Quantification of the p-IκBα/IκBα expression level in mouse skin. (D) Protein expression levels of IκBα quantified by densitometric analysis. (E) Quantification of the p-p65/p65 expression level ratio in mouse skin. Protein expression levels of (F) p65, (G) acetyl-p65 and (H) SIRT1 quantified by densitometric analysis. Data were presented as mean ± standard deviation (n=4). $^{\#\#}$P<0.01, $^{\#\#\#}$P<0.001 vs. sham group; *P<0.05, **P<0.01, ***P<0.001 vs. model group. CI_{SCFE}, supercritical carbon dioxide fluid extraction of *Chrysanthemum indicum* Linnén; NAA, nicotinamide; L, low dose; H, high dose; p, phosphorylated; SIRT1, NAD-dependent protein deacetylase sirtuin-1.

The clinical manifestations of cSCC may present as small spots and nodules in the early stages of disease, followed by necrosis, ulceration or mycosis, which can present as flat ulcers with raised edges and are accompanied by scaling (38). In the present study, the mice demonstrated clinical manifestations similar to those of cSCC after 31 weeks of UV irradiation. In addition, the diagnosis of skin cancer needs to be combined with histopathological analysis (39). The pathological results of the present study showed abnormal proliferation of the epidermis into the deep dermis in the model mouse group, in addition to increased inflammatory cell infiltration, which is consistent with previously published literature (40,41). The results of the present study suggested that CI_{SCFE} treatment may effectively inhibit the development of UV-induced skin cancer in mice.

The anticancer effects of CI_{SCFE} in the present study may be closely related to the biological activities of its chemical components. The chemical compositions of CI_{SCFE} analyzed using GC-MS (Table SI) showed that the main components were d-camphor, β-caryophyllene and thymol, which exhibit

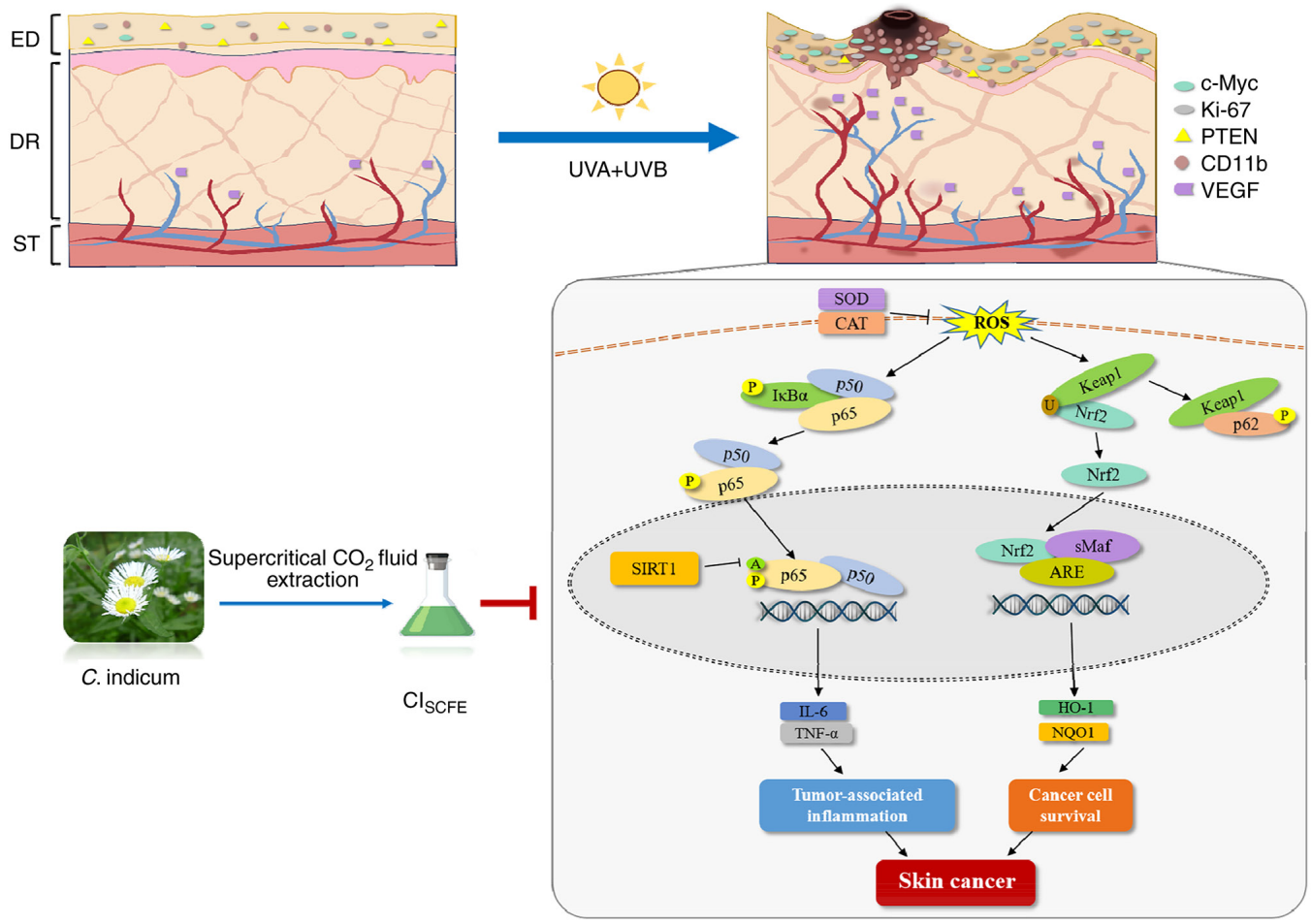

Figure 8. Summary schema of the protective mechanism of CI_{SCFE} against UV-induced skin carcinogenesis. CI_{SCFE}, supercritical carbon dioxide fluid extraction of *C. indicum*; SOD, superoxide dismutase; CAT, catalase; ROS, reactive oxygen species; Keap1, Kelch-like ECH associated protein 1; Nrf2, nuclear factor 2 erythroid 2-related factor 2; SIRT1, NAD-dependent protein deacetylase sirtuin-1; HO-1, heme oxygenase 1; NQO1, NAD(P)H dehydrogenase [quinone] 1; P, phosphorylated; A, acetylated; U, ubiquitinated; *C. indicum*, *Chrysanthemum indicum* Linnén; sMaf, small musculoaponeurotic fibrosarcoma; ARE, antioxidant response elements; ED, epidermis; DR, dermis; ST, subcutaneous tissue.

anti-inflammatory and antioxidant capabilities (42-44). In addition, caryophyllene oxide and thymol were reported to have antitumor activities (45,46). Eucalyptol may inhibit skin carcinogenesis *in vivo* and *in vitro* by reducing the migration and invasion of cancer cells (43). HPLC analysis was used to quantify four constituents in the present study, which were chlorogenic acid, linarin, luteolin-7-glucoside and luteolin. Chlorogenic acid and linarin inhibit the NF-κB signaling pathway and thereby inhibit cancer cell growth and proliferation (47,48). A previous study reported that lignan-7-glucoside inhibited the migration and invasion of oral cancer cells by regulating matrix metalloproteinase-2 expression and the extracellular signal-regulated kinase pathway (49). Luteolin has also been reported to act as an anti-inflammatory and anticancer agent (50). It could therefore be suggested that the active compounds in CI_{SCFE}, particularly the active components with potential anti-inflammatory and anticancer effects, may be key to the prevention and treatment of skin cancer using CI_{SCFE}. Therefore, it was investigated whether CI_{SCFE} inhibited UV-induced skin cancer in mice by exerting antioxidant and anti-inflammatory effects.

The activation of oncogenes and suppression of anti-oncogenes are important for determining carcinogenesis (51). c-Myc is a recognized oncogenic gene and its variants are observed in >70% of human cancers (52). Pelengaris *et al* (53) reported that sustained activation of c-Myc can induce abnormal skin hyperplasia, related keratinization insufficiency and angiogenesis. The hyperplastic epidermis was found to be accompanied by the expression of Ki-67, which serves as an attractive prognostic, predictive and potential therapeutic target for malignancies (54). Tumors are often associated with vascular dilation and proliferation, which provides adequate oxygen and nutrients to the cancer cells for proliferation (55). VEGF is crucial in skin angiogenesis and its abnormal activation within tumors causes the blood vessels in and around the tumor to grow exponentially (56). In the present study, the expression levels of c-Myc, VEGF and Ki-67 were increased following UV irradiation, which led to vasodilation in the dermis and hyperplasia in the epidermis. PTEN, a common mutant tumor suppressor gene, has exhibited inactivation or partial loss of function in numerous types of cancer (57). It has been reported that long-term UV irradiation causes genetic alterations in PTEN and reduces its expression level (58). In the present study, it was demonstrated that CI_{SCFE} reduced the expression levels of c-Myc, VEGF and Ki-67 and

restored that of PTEN, thereby potentially alleviating skin cancer progression.

Long-term UV exposure can cause oxidative imbalance and lead to the accumulation of ROS, which induces a series of signal transduction events contributing to inflammatory immune imbalance, DNA injury and even cancer (59). Excessive accumulation of ROS can be detected through measuring levels of 8-OHdG, a biomarker of oxidative DNA damage (60). Moreover, 8-OHdG has been reported to be elevated in a number of types of cancer, such as colorectal, gastric and melanoma skin cancers (61,62). SOD and CAT serve a crucial role in the cellular antioxidant system, reducing the oxidative induction of proto-oncogenes and structural DNA damage by oxidative carcinogens (63). In the present study, CI_{SCFE} reduced the excessive production of ROS and oxidative DNA damage induced by UV and restored the activities of antioxidants including SOD and CAT. Moreover, the inflammatory factors induced by UV can also contribute to the progression of skin cancer and CD11b may be expressed in various types of inflammatory cells, which can be used to determine inflammatory injury (64). Previous studies have reported that photo-carcinogenesis is associated with UV-induced infiltration of CD11b cell populations and CD11b-mediated oxidative damage (65). Reduction of UV-induced infiltration of CD11b+ cells can prevent UV-induced skin aging and skin cancer (66). In the present study, increased CD11b expression was demonstrated in mouse skin tumors, and IL-6 and TNF-α protein expression levels were increased. However, CI_{SCFE} reduced the UV-induced infiltration of inflammatory cells, the protein expression levels of IL-6 and TNF-α and the number of CD11b cells. Therefore, CI_{SCFE} may potentially prevent skin cancer by inhibiting inflammation and oxidative stress induced by UV.

Nrf2 activation is beneficial to the survival of precancerous or cancer cells because oncogene mutations provide these cells with a higher proliferative capacity and viability by upregulating Nrf2 expression (67). Kim *et al* (68) reported that the mutation and sustained activation of Nrf2 affected the differentiation of squamous epithelial cells and was ubiquitous in cSCC. Moreover, p62 has been reported to be involved in the activation of Nrf2 in cancer cells. P62 competes with Nrf2 for the Keap1 binding site, especially when p62 is phosphorylated at serine 349 (Ser-349) (69). Keap1 is subsequently degraded and Nrf2 is released, leading to its persistent activation and subsequent transfer to the nucleus to exert its effect (16,70). In the present study, prolonged UV irradiation increased the expression level of Nrf2, p62 phosphorylation at Serine 349 (Ser-349) and increased the expression levels of downstream proteins NQO1 and HO-1. However, CI_{SCFE} treatment diminished the UV-induced expression of p-p62 and reduced the continuous expressions of Nrf2 and downstream NQO1 and HO-1, thereby potentially inhibiting the development of skin cancer.

The expression of NF-κB is triggered in tumor cells and cells that constitute the tumor microenvironment, promoting the production of cytokines and ultimately activating genes involved in abnormal growth and malignant tumor expression (71). Nrf2 and activated antioxidant enzymes, such as HO-1, inhibit the NF-κB pathway, thereby reducing inflammatory damage (72). However, CI_{SCFE} in the present UV-induced mouse skin cancer model did not inhibit NF-κB expression via the Nrf2/HO-1 pathway, but instead potentially inhibited NF-κB expression via SIRT1. A number of previous studies have reported that NF-κB is present in the cytoplasm as a p50/RelA (p65) dimer or RelB/p52 dimer. SIRT1 can deacetylate lysine 310 of p65 to inhibit the transcription of inflammation-related genes (73-76). The present study indicated that UV irradiation decreased the protein expression levels of SIRT1, which is in accordance with the previous study by Ming *et al* (76) in which the level of SIRT1 in patients with UV-related skin cancer was reduced. Moreover, the present study found that UV radiation increased the acetylation and phosphorylation of p65 to activate NF-κB. CI_{SCFE} increased SIRT1 protein expression levels and inhibited the activation of the NF-κB pathway, thereby potentially reducing the occurrence of skin inflammation, and even cancer.

In summary, CI_{SCFE} exhibited potent anti-inflammatory and anti-skin cancer activity (Fig. 8). CI_{SCFE} inhibited UV-induced epidermal abnormal proliferation and dermal fiber damage, reducing epidermal cell carcinogenesis. CI_{SCFE} also suppressed oxidative stress and the inflammatory response in mouse skin. CI_{SCFE} enhanced the protein expression level of SIRT1, which suppressed the abnormal activation of the pro-inflammatory factor NF-κB. Moreover, CI_{SCFE} reduced the protein expression level of p62, which reduced the abnormal activation of Nrf2. Therefore, the potential effect of CI_{SCFE} on skin cancer may be related to its anti-inflammatory and antioxidant chemical compositions. These findings suggested that CI_{SCFE} may potentially be a future prospective drug for the prevention and therapy of UV-induced skin cancer. However, the present study evaluated the anti-UV-induced skin cancer effects of CI_{SCFE} in mice and was not evaluated in patients with skin cancer. In future studies, the therapeutic effects of CI_{SCFE} should be studied in patients with skin cancer. In addition, the present study evaluated the expression levels of CD11b, which is commonly used as a biomarker for NK cells, monocytes, dendritic cells and neutrophils (77-80). B cells and T cells are also important classes of immune cells that serve an important role in skin inflammation and skin cancer progression (81,82). In future studies, the relationship between T cells and B cells and the progression of skin cancer should be examined.

Acknowledgments

Not applicable.

Funding

The present study was funded by The Science and Technology Planning Project of Guangzhou (grant no. 202102021263).

Availability of data and materials

The data generated in the present study may be requested from the corresponding author.

Authors' contributions

YXZ and BQL developed and designed the study concept. QHL, QYZ, HJC, HEH, YQH, YCL, BL, YQW and SLD

conducted the experiments and collected data. QHL, QYZ and HJC interpreted the results and drafted the manuscript. BQL, XHD and YXZ analyzed data and confirm the authenticity of all the raw data. All authors have read and approved the final version of the manuscript.

Ethics approval and consent to participate

The present study was conducted according to the guidelines of the Animal Care and Use Committee of Guangzhou University of Chinese Medicine (approval no. 20190304024; Guangzhou, China).

Patient consent for publication

Not applicable.

Competing interests

The authors declare that they have no competing interests.

References

1. Sung H, Ferlay, J, Siegel RL, Laversanne M, Soerjomataram I, Jemal A and Bray F: Global cancer statistics 2020: GLOBOCAN estimates of incidence and mortality worldwide for 36 cancers in 185 countries. CA Cancer J Clin 71: 209-249, 2021.
2. Burton KA, Ashack KA and Khachemoune A: Cutaneous squamous cell carcinoma: A review of high-risk and metastatic disease. Am J Clin Dermatol 17: 491-508, 2016.
3. Rogers HW, Weinstock MA, Feldman SR and Coldiron BM: Incidence estimate of nonmelanoma skin cancer (keratinocyte carcinomas) in the U.S. population, 2012. JAMA Dermatol 151: 1081-1086, 2015.
4. Bachelor MA and Bowden GT: UVA-mediated activation of signaling pathways involved in skin tumor promotion and progression. Semin Cancer Biol 14: 131-138, 2004.
5. Winge MCG, Kellman LN, Guo K, Tang JY, Swetter SM, Aasi SZ, Sarin KY, Chang ALS and Khavari PA: Advances in cutaneous squamous cell carcinoma. Nat Rev Cancer 23: 430-449, 2023.
6. Forrester SJ, Kikuchi DS, Hernandes MS, Xu Q and Griendling KK: Reactive oxygen species in metabolic and inflammatory signaling. Circ Res 122: 877-902, 2018.
7. Singh A, Kukreti R, Saso L and Kukreti S: Mechanistic insight into oxidative stress-triggered signaling pathways and type 2 diabetes. Molecules 27: 950, 2022.
8. Kim YE and Kim J: ROS-scavenging therapeutic hydrogels for modulation of the inflammatory response. ACS Appl Mater Interfaces: Dec 28, 2021 (Epub ahead of print).
9. Aggarwal V, Tuli HS, Varol A, Thakral F, Yerer MB, Sak K, Varol M, Jain A, Khan MA and Sethi G: Role of reactive oxygen species in cancer progression: molecular mechanisms and recent advancements. Biomolecules 9: 735, 2019.
10. Kawanishi S, Ohnishi S, Ma N, Hiraku Y and Murata M: Crosstalk between DNA damage and inflammation in the multiple steps of carcinogenesis. Int J Mol Sci 18: 1808, 2017.
11. Jomova K, Raptova R, Alomar SY, Alwasel SH, Nepovimova E, Kuca K and Valko M: Reactive oxygen species, toxicity, oxidative stress, and antioxidants: Chronic diseases and aging. Arch Toxicol 97: 2499-2574, 2023.
12. Zhao Y, Ye X, Xiong Z, Ihsan A, Ares I, Martínez M, Lopez-Torres B, Martínez-Larrañaga MR, Anadón A, Wang X and Martínez MA: Cancer metabolism: the role of ROS in DNA damage and induction of apoptosis in cancer cells. Metabolites 13: 796, 2023.
13. Jaramillo MC and Zhang DD: The emerging role of the Nrf2-Keap1 signaling pathway in cancer. Genes Dev 27: 2179-2191, 2013.
14. Kitamura H and Motohashi H: NRF2 addiction in cancer cells. Cancer Sci 109: 900-911, 2018.
15. He F, Antonucci L and Karin M: NRF2 as a regulator of cell metabolism and inflammation in cancer. Carcinogenesis 41: 405-416, 2020.
16. Ichimura Y, Waguri S, Sou YS, Kageyama S, Hasegawa J, Ishimura R, Saito T, Yang Y, Kouno T, Fukutomi T, *et al*: Phosphorylation of p62 activates the Keap1-Nrf2 pathway during selective autophagy. Mol Cell 51: 618-631, 2013.
17. Singh V and Ubaid S: Role of silent information regulator 1 (SIRT1) in regulating oxidative stress and inflammation. Inflammation 43: 1589-1598, 2020.
18. Jiang SB, Lu YS, Liu T, Li LM, Wang HX, Wu Y, Gao XH and Chen HD: UVA influenced the SIRT1-miR-27a-5p-SMAD2-MMP1/COL1/BCL2 axis in human skin primary fibroblasts. J Cell Mol Med 24: 10027-10041, 2020.
19. Wu P, Zhang B, Han X, Sun Y, Sun Z, Li L, Zhou X, Jin Q, Fu P, Xu W and Qian H: HucMSC exosome-delivered 14-3-3ζ alleviates ultraviolet radiation-induced photodamage via SIRT1 pathway modulation. Aging 13: 11542-11563, 2021.
20. Valente S, Mellini P, Spallotta F, Carafa V, Nebbioso A, Polletta L, Carnevale I, Saladini S, Trisciuoglio D, Gabellini C, *et al*: 1,4-Dihydropyridines active on the SIRT1/AMPK pathway ameliorate skin repair and mitochondrial function and exhibit inhibition of proliferation in cancer cells. J Med Chem 59: 1471-1491, 2016.
21. Puppala ER, Yalamarthi SS, Aochenlar SL, Prasad N, Syamprasad NP, Singh M, Nanjappan SK, Ravichandiran V, Tripathi DM, Gangasani JK and Naidu VGM: Mesua assamica (King&Prain) kosterm. Bark ethanolic extract attenuates chronic restraint stress aggravated DSS-induced ulcerative colitis in mice via inhibition of NF-κB/STAT3 and activation of HO-1/Nrf2/SIRT1 signaling pathways. J Ethnopharmacol 301: 115765, 2023.
22. Zhang X, Wu JZ, Lin ZX, Yuan QJ, Li YC, Liang JL, Zhan JY, Xie YL, Su ZR and Liu YH: Ameliorative effect of supercritical fluid extract of *Chrysanthemum indicum* Linnén against D-galactose induced brain and liver injury in senescent mice via suppression of oxidative stress, inflammation and apoptosis. J Ethnopharmacol 234: 44-56, 2019.
23. Shao Y, Sun Y, Li D and Chen Y: *Chrysanthemum indicum* L.: A comprehensive review of its botany, phytochemistry and pharmacology. Am J Chin Med 48: 871-897, 2020.
24. Kim WJ, Yu HS, Bae WY, Ko KY, Chang KH, Lee NK and Paik HD: *Chrysanthemum indicum* suppresses adipogenesis by inhibiting mitotic clonal expansion in 3T3-L1 preadipocytes. J Food Biochem 45: e13896, 2021.
25. Yang X, Liu Y, Zhong C, Hu J, Xu S, Zhang P and He L: Total flavonoids of *Chrysanthemum indicum* L inhibit acute pancreatitis through suppressing apoptosis and inflammation. BMC Complement Med Ther 23: 23, 2023.
26. Wu XL, Li CW, Chen HM, Su ZQ, Zhao XN, Chen JN, Lai XP, Zhang XJ and Su ZR: Anti-inflammatory effect of supercritical-carbon dioxide fluid extract from flowers and buds of *Chrysanthemum indicum* Linnen. Evid Based Complement Alternat Med 2013: 413237: 2013.
27. Yang HM, Sun CY, Liang JL, Xu LQ, Zhang ZB, Luo DD, Chen HB, Huang YZ, Wang Q, Lee DY, *et al*: Supercritical-carbon dioxide fluid extract from *Chrysanthemum indicum* enhances anti-tumor effect and reduces toxicity of bleomycin in tumor-bearing mice. Int J Mol Sci 18: 465, 2017.
28. Zhang X, Xie YL, Yu XT, Su ZQ, Yuan J, Li YC, Su ZR, Zhan JY and Lai XP: Protective effect of super-critical carbon dioxide fluid extract from flowers and buds of *Chrysanthemum indicum* Linnén against ultraviolet-induced photo-aging in mice. Rejuvenation Res 18: 437-448, 2015.
29. MacArthur Clark JA and Sun D: Guidelines for the ethical review of laboratory animal welfare people's republic of china national standard GB/T 35892-2018 [Issued 6 February 2018 Effective from 1 September 2018]. Animal Model Exp Med 3: 103-113, 2020.
30. Pillon A, Gomes B, Vandenberghe I, Cartron V, Cèbe P, Blanchet JC, Sibaud V, Guilbaud N, Audoly L, Lamant L and Kruczynski A: Actinic keratosis modelling in mice: A translational study. PLoS One 12: e0179991, 2017.
31. Zhong QY, Lin B, Chen YT, Huang YP, Feng WP, Wu Y, Long GH, Zou YN, Liu Y, Lin BQ, *et al*: Gender differences in UV-induced skin inflammation, skin carcinogenesis and systemic damage. Environ Toxicol Pharmacol 81: 103512, 2021.
32. Wang Y, Zhao Z, Jiao W, Yin Z, Zhao W, Bo H, Bi Z, Dong B, Chen B and Wang Z: PRAF2 is an oncogene acting to promote the proliferation and invasion of breast cancer cells. Exp Ther Med 24: 738, 2022.
33. Que SKT, Zwald FO and Schmults CD: Cutaneous squamous cell carcinoma: Incidence, risk factors, diagnosis, and staging. J Am Acad Dermatol 78: 237-247, 2018.

34. Sun S, Jiang P, Su W, Xiang Y, Li J, Zeng L and Yang S: Wild chrysanthemum extract prevents UVB radiation-induced acute cell death and photoaging. Cytotechnology 68: 229-240, 2016.
35. Allen NC, Martin AJ, Snaidr VA, Eggins R, Chong AH, Fernandéz-Peñas P, Gin D, Sidhu S, Paddon VL, Banney LA, *et al*: Nicotinamide for skin-cancer chemoprevention in transplant recipients. N Engl J Med 388: 804-812, 2023.
36. Snaidr VA, Damian DL and Halliday GM: Nicotinamide for photoprotection and skin cancer chemoprevention: A review of efficacy and safety. Exp Dermatol 28 (Suppl 1): S15-S22, 2019.
37. Damian DL: Nicotinamide for skin cancer chemoprevention. Australas J Dermatol 58: 174-180, 2017.
38. Stratigos A, Garbe C, Lebbe C, Malvehy J, del Marmol V, Pehamberger H, Peris K, Becker JC, Zalaudek I, Saiag P, *et al*: Diagnosis and treatment of invasive squamous cell carcinoma of the skin: European consensus-based interdisciplinary guideline. Eur J Cancer 51: 1989-2007, 2015.
39. Stratigos AJ, Garbe C, Dessinioti C, Lebbe C, Bataille V, Bastholt L, Dreno B, Fargnoli MC, Forsea AM, Frenard C, *et al*: European interdisciplinary guideline on invasive squamous cell carcinoma of the skin: Part 1. Epidemiology, diagnostics and prevention. Eur J Cancer 128: 60-82, 2020.
40. Dorrell DN and Strowd LC: Skin cancer detection technology. Dermatol Clin 37: 527-536, 2019.
41. Firnhaber JM: Basal cell and cutaneous squamous cell carcinomas: Diagnosis and treatment. Am Fam Physician 102: 339-346, 2020.
42. Wang X, Liu Y, Niu Y, Wang N and Gu W: The chemical composition and functional properties of essential oils from four species of Schisandra growing wild in the qinling mountains, China. Molecules 23: 1645, 2018.
43. Rahaman A, Chaudhuri A, Sarkar A, Chakraborty S, Bhattacharjee S and Mandal DP: Eucalyptol targets PI3K/Akt/mTOR pathway to inhibit skin cancer metastasis. Carcinogenesis 43: 571-583, 2022.
44. Rawat A, Rawat M, Prakash OM, Kumar R, Punetha H and Rawat DS: Comparative study on eucalyptol and camphor rich essential oils from rhizomes of Hedychium spicatum Sm. and their pharmacological, antioxidant and antifungal activities. An Acad Bras Cienc 94: e20210932, 2022.
45. Li Y, Wen JM, Du CJ, Hu SM, Chen JX, Zhang SG, Zhang N, Gao F, Li SJ, Mao XW, *et al*: Thymol inhibits bladder cancer cell proliferation via inducing cell cycle arrest and apoptosis. Biochem Biophys Res Commun 491: 530-536, 2017.
46. Xiu Z, Zhu Y, Han J, Li Y, Yang X, Yang G, Song G, Li S, Li Y, Cheng C, *et al*: Caryophyllene oxide induces ferritinophagy by regulating the NCOA4/FTH1/LC3 pathway in hepatocellular carcinoma. Front Pharmacol 13: 930958, 2022.
47. Zhen ZG, Ren SH, Ji HM, Ma JH, Ding XM, Feng FQ, Chen SL, Zou P, Ren JR and Jia L: Linarin suppresses glioma through inhibition of NF-κB/p65 and up-regulating p53 expression in vitro and in vivo. Biomed Pharmacother 95: 363-374, 2017.
48. Wang L, Du H and Chen P: Chlorogenic acid inhibits the proliferation of human lung cancer A549 cell lines by targeting annexin A2 in vitro and in vivo. Biomed Pharmacother 131: 110673, 2020.
49. Velmurugan BK, Lin JT, Mahalakshmi B, Chuang YC, Lin CC, Lo YS, Hsieh MJ and Chen MK: Luteolin-7-O-glucoside inhibits oral cancer cell migration and invasion by regulating matrix metalloproteinase-2 expression and extracellular signal-regulated kinase pathway. Biomolecules 10: 502, 2020.
50. Singh S, Gupta P, Meena A and Luqman S: Acacetin, a flavone with diverse therapeutic potential in cancer, inflammation, infections and other metabolic disorders. Food Chem Toxicol 145: 111708, 2020.
51. Weinstein IB and Joe A: Oncogene addiction. Cancer Res 68: 3077-3080, 2008.
52. Wu H, Yang TY, Li Y, Ye WL, Liu F, He XS, Wang JR, Gan WJ, Li XM, Zhang S, *et al*: Tumor necrosis factor receptor-associated factor 6 promotes hepatocarcinogenesis by interacting with histone deacetylase 3 to enhance c-Myc gene expression and protein stability. Hepatology 71: 148-163, 2020.
53. Pelengaris S, Littlewood T, Khan M, Elia G and Evan G: Reversible activation of c-Myc in skin: Induction of a complex neoplastic phenotype by a single oncogenic lesion. Mol Cell 3: 565-577, 1999.
54. Menon SS, Guruvayoorappan C, Sakthivel KM and Rasmi RR: Ki-67 protein as a tumour proliferation marker. Clin Chim Acta 491: 39-45, 2019.
55. Viallard C and Larrivée B: Tumor angiogenesis and vascular normalization: Alternative therapeutic targets. Angiogenesis 20: 409-426, 2017.
56. Carmeliet P: VEGF as a key mediator of angiogenesis in cancer. Oncology 69 (Suppl 3): S4-S10, 2005.
57. Álvarez-Garcia V, Tawil Y, Wise HM and Leslie NR: Mechanisms of PTEN loss in cancer: It's all about diversity. Semin Cancer Biol 59: 66-79, 2019.
58. Wang Y, Digiovanna JJ, Stern JB, Hornyak TJ, Raffeld M, Khan SG, Oh KS, Hollander MC, Dennis PA and Kraemer KH: Evidence of ultraviolet type mutations in xeroderma pigmentosum melanomas. Proc Natl Acad Sci USA 106: 6279-6284, 2009.
59. Garg C, Sharma H and Garg M: Skin photo-protection with phytochemicals against photo-oxidative stress, photocarcinogenesis, signal transduction pathways and extracellular matrix remodeling-An overview. Ageing Res Rev 62: 101127, 2020.
60. Al-Sadek T and Yusuf N: Ultraviolet radiation biological and medical implications. Curr Issues Mol Biol 46: 1924-1942, 2024.
61. Jelic MD, Mandic AD, Maricic SM and Srdjenovic BU: Oxidative stress and its role in cancer. J Cancer Res Ther 17: 22-28, 2021.
62. Murtas D, Piras F, Minerba L, Ugalde J, Floris C, Maxia C, Demurtas P, Perra MT and Sirigu P: Nuclear 8-hydroxy-2'-deoxyguanosine as survival biomarker in patients with cutaneous melanoma. Oncol Rep 23: 329-335, 2010.
63. Cerutti P, Ghosh R, Oya Y and Amstad P: The role of the cellular antioxidant defense in oxidant carcinogenesis. Environ Health Perspect 102 (Suppl 10): S123-S129, 1994.
64. Sluyter R and Halliday GM: Infiltration by inflammatory cells required for solar-simulated ultraviolet radiation enhancement of skin tumor growth. Cancer Immunol Immunother 50: 151-156, 2001.
65. Mittal A, Elmets CA and Katiyar SK: CD11b+ cells are the major source of oxidative stress in UV radiation-irradiated skin: possible role in photoaging and photocarcinogenesis. Photochem Photobiol 77: 259-264, 2003.
66. Katiyar SK, Meleth S and Sharma SD: Silymarin, a flavonoid from milk thistle (Silybum marianum L.), inhibits UV-induced oxidative stress through targeting infiltrating CD11b+ cells in mouse skin. Photochem Photobiol 84: 266-271, 2008.
67. Su H, Yang F, Fu R, Li X, French R, Mose E, Pu X, Trinh B, Kumar A, Liu J, *et al*: Cancer cells escape autophagy inhibition via NRF2-induced macropinocytosis. Cancer Cell 39: 678-693. e11, 2021.
68. Kim YR, Oh JE, Kim MS, Kang MR, Park SW, Han JY, Eom HS, Yoo NJ and Lee SH: Oncogenic NRF2 mutations in squamous cell carcinomas of oesophagus and skin. J Pathol 220: 446-451, 2010.
69. Jiang T, Harder B, Rojo de la Vega M, Wong PK, Chapman E and Zhang DD: p62 links autophagy and Nrf2 signaling. Free Radic Biol Med 88: 199-204, 2015.
70. Lee DH, Park JS, Lee YS, Han J, Lee DK, Kwon SW, Han DH, Lee YH and Bae SH: SQSTM1/p62 activates NFE2L2/NRF2 via ULK1-mediated autophagic KEAP1 degradation and protects mouse liver from lipotoxicity. Autophagy 16: 1949-1973, 2020.
71. Inoue J, Gohda J, Akiyama T and Semba K: NF-kappaB activation in development and progression of cancer. Cancer Sci 98: 268-274, 2007.
72. Bellezza I, Giambanco I, Minelli A and Donato R: Nrf2-Keap1 signaling in oxidative and reductive stress. Biochim Biophys Acta Mol Cell Res 1865: 721-733, 2018.
73. Li CX, Gao JG, Wan XY, Chen Y, Xu CF, Feng ZM, Zeng H, Lin YM, Ma H, Xu P, *et al*: Allyl isothiocyanate ameliorates lipid accumulation and inflammation in nonalcoholic fatty liver disease via the Sirt1/AMPK and NF-κB signaling pathways. World J Gastroenterol 25: 5120-5133, 2019.
74. Chen M, Chen Z, Huang D, Sun C, Xie J, Chen T, Zhao X, Huang Y, Li D, Wu B and Wu D: Myricetin inhibits TNF-α-induced inflammation in A549 cells via the SIRT1/NF-κB pathway. Pulm Pharmacol Ther 65: 102000, 2020.
75. Sun HJ, Xiong SP, Cao X, Cao L, Zhu MY, Wu ZY and Bian JS: Polysulfide-mediated sulfhydration of SIRT1 prevents diabetic nephropathy by suppressing phosphorylation and acetylation of p65 NF-κB and STAT3. Redox Biol 38: 101813, 2021.
76. Ming M, Shea CR, Guo X, Li X, Soltani K, Han W and He YY: Regulation of global genome nucleotide excision repair by SIRT1 through xeroderma pigmentosum C. Proc Natl Acad Sci USA 107: 22623-22628, 2010.

77. Scott NR, Swanson RV, Al-Hammadi N, Domingo-Gonzalez R, Rangel-Moreno J, Kriel BA, Bucsan AN, Das S, Ahmed M, Mehra S, *et al*: S100A8/A9 regulates CD11b expression and neutrophil recruitment during chronic tuberculosis. J Clin Invest 130: 3098-3112, 2020.
78. Crinier A, Narni-Mancinelli E, Ugolini S and Vivier E: SnapShot: Natural killer cells. Cell 180: 1280-1280.e1, 2020.
79. Subhi Y, Krogh Nielsen M, Molbech CR, Krüger Falk M, Singh A, Hviid TVF, Nissen MH and Sørensen TL: Association of CD11b+ monocytes and anti-vascular endothelial growth factor injections in treatment of neovascular age-related macular degeneration and polypoidal choroidal vasculopathy. JAMA Ophthalmol 137: 515-522, 2019.
80. Rombouts M, Ammi R, Van Brussel I, Roth L, De Winter BY, Vercauteren SR, Hendriks JM, Lauwers P, Van Schil PE, De Meyer GR, *et al*: Linking CD11b (+) dendritic cells and natural killer T cells to plaque inflammation in atherosclerosis. Mediators Inflamm 2016: 6467375, 2016.
81. Sluyter R and Halliday GM: Enhanced tumor growth in UV-irradiated skin is associated with an influx of inflammatory cells into the epidermis. Carcinogenesis 21: 1801-1807, 2000.
82. Scibiorek M, Mthembu N, Mangali S, Ngomti A, Ikwegbue P, Brombacher F and Hadebe S: IL-4Rα signalling in B cells and T cells play differential roles in acute and chronic atopic dermatitis. Sci Rep 13: 144, 2023.